Multifunctional Polymeric Micelles as Cancer-Targeted, MRI-Ultrasensitive Drug Delivery Systems

Norased Nasongkla,[†] Erik Bey,[†] Jimin Ren,[‡] Hua Ai,[†] Chalermchai Khemtong,[†] Jagadeesh Setti Guthi,[†] Shook-Fong Chin,[†] A. Dean Sherry,[‡] David A. Boothman,[†] and Jinming Gao*,[†]

Simmons Comprehensive Cancer Center, University of Texas Southwestern Medical Center at Dallas, 5323 Harry Hines Boulevard, Dallas, Texas 75390, and Advanced Imaging Research Center, University of Texas Southwestern Medical Center at Dallas, 5323 Harry Hines Boulevard, Dallas, Texas 75390
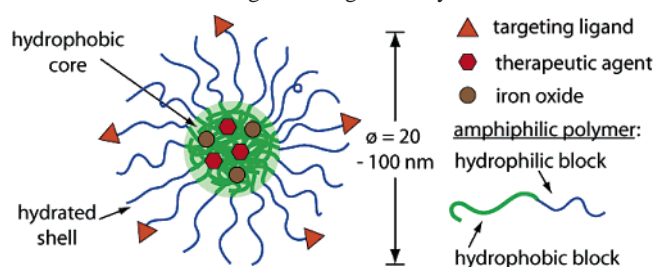
ABSTRACT

We describe the development of multifunctional polymeric micelles with cancer-targeting capability via $\alpha_v\beta_3$ integrins, controlled drug delivery, and efficient magnetic resonance imaging (MRI) contrast characteristics. Doxorubicin and a cluster of superparamagnetic iron oxide (SPIO) nanoparticles were loaded successfully inside the micelle core. The presence of cRGD on the micelle surface resulted in the cancer-targeted delivery to $\alpha_v\beta_3$-expressing tumor cells. In vitro MRI and cytotoxicity studies demonstrated the ultrasensitive MRI imaging and $\alpha_v\beta_3$-specific cytotoxic response of these multifunctional polymeric micelles.

Over the past several years, we have witnessed an explosive development of nanomedicine platforms in drug delivery and molecular imaging applications.[1,2] Nanoscopic therapeutic systems that incorporate therapeutic agents, molecular targeting, and diagnostic imaging capabilities are emerging as the next generation of multifunctional nanomedicine to improve the therapeutic outcome of drug therapy (Scheme 1). Among the many nanoparticulate systems, polymeric micelles, self-assembled nanoparticles from amphiphilic block copolymers, provide a unique core–shell architecture wherein the hydrophobic core serves as a natural carrier environment for hydrophobic drugs and the hydrophilic shell allows particle stabilization in aqueous solution.[3–5] Sterically stabilized micelles by the PEG corona have shown prolonged blood circulation and "passive" targeting of micelles to solid tumors through the enhanced permeability and retention (EPR) effect, leading to Phase I clinical trials of several micellar systems in cancer patients.[6–8] Although the leaky vasculature of solid tumors enhances micelle accumulation in tumor tissues, significant micelle uptake in reticuloendothelial systems such as liver and spleen has also been observed.[9] To further improve delivery efficiency and cancer specificity, a strong impetus has been placed on the development of micellar systems that can *actively* target tumors through

Scheme 1. Multifunctional Nanomedicine Platform for Targeted Drug Delivery


molecular recognition of unique cancer-specific markers. Integrin $\alpha_v\beta_3$ is such a molecular target that is highly expressed in angiogenic endothelial cells in many solid tumors.[10] Various $\alpha_v\beta_3$-targeted therapeutic systems have shown remarkable in vitro and in vivo success.[11,12]

In this study, we describe the development of multifunctional polymeric micelles with cancer-targeting capability for controlled drug delivery and efficient magnetic resonance imaging (MRI) contrast characteristics. These novel micelles are composed of three key components: (1) a chemotherapeutic agent doxorubicin (DOXO) that is released from polymeric micelles through a pH-dependent mechanism; (2) a cRGD ligand that can target $\alpha_v\beta_3$ integrins on tumor endothelial cells and subsequently induce receptor-mediated endocytosis for cell uptake; and (3) a cluster of superparamagnetic iron oxide (SPIO) nanoparticles that is loaded inside

* Corresponding author. E-mail: jinming.gao@utsouthwestern.edu. Phone: (+1) 214-648-9278. Fax: (+1) 214-648-0264.
† Simmons Comprehensive Cancer Center.
‡ Advanced Imaging Research Center.
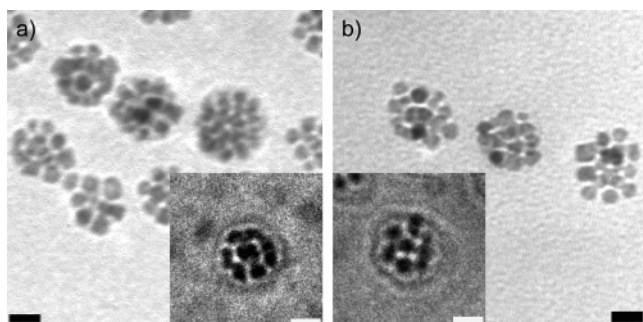
Figure 1. Transmission electron microscopy (TEM) images of (a) 0% cRGD- and (b) 16% cRGD-DOXO-SPIO-loaded polymeric micelles. The insets show the cryo-TEM images from the same micelle samples. The scale bars are 20 nm in all images.

the hydrophobic core of each micelle for ultrasensitive MRI detection.

Hydrophobic, monodisperse SPIO nanoparticles (8 nm in diameter) were first synthesized following a published procedure.[13] Subsequently, SPIO and DOXO were loaded into the polymeric micelles by a solvent-evaporation method[14] at 6.7 and 2.7 w/w %, respectively. In this study, amphiphilic block copolymers of maleimide-terminated poly(ethylene glycol)-block-poly(D,L-lactide) (MAL-PEG-PLA, M_n =7.2 kD, M_n(PEG) = 3.2 kD) and methoxy-terminated poly-(ethylene glycol)-block-poly(D,L-lactide) copolymer (MPEG-PLA, M_n = 6.4 kD, M_n(PEG) = 2.0 kD) were used for micelle formation. Different amounts of MPEG-PLA were introduced to control the density of maleimide, which ultimately determined the density of cRGD on the micelle surface (0 and 16% of all PEG chains). cRGD was attached to the micelle surface through a covalent thiol−maleimide linkage (see the Supporting Information). The residual maleimide groups were quenched by reaction with cysteine and dialyzed before the subsequent studies.

Bright-field transmission electron microscopy (TEM) shows the morphology of SPIO-DOX-loaded, cRGD-free (0%) (Figure 1a) and cRGD-encoded (16%) PEG-PLA micelles (Figure 1b). Because PEG-PLA copolymer and DOXO do not significantly attenuate electron beams under TEM, SPIO-loaded micelles are largely present as isolated clusters of SPIO nanoparticles. Figure insets show the cryogenic TEM (cryo-TEM) images of both samples. Compared to bright-field TEM where samples were dried on a solid carbon-coated grid, cryo-TEM preserved the size and morphology of micelle nanoparticles in the hydrated state. Cryo-TEM measurements showed that micelle diameters are 47 ± 4 and 45 ± 8 nm for 0% and 16% cRGD-SPIO-DOX micelles (n = 30 for each sample), respectively. Dynamic light scattering (DLS) showed that the micelle diameters are 46 ± 5 and 46 ± 4 nm for 0% and 16% cRGD-SPIO-DOX micelles, respectively. With either method, we did not observe statistically significant differences between the cRGD-functionalized versus cRGD-free SPIO-DOXO micelles.

The clustering of SPIO nanoparticles inside micelle cores has demonstrated the dramatic increase of the T_2 relaxivity (per Fe) and the high loading density of SPIO (up to 50 w/w
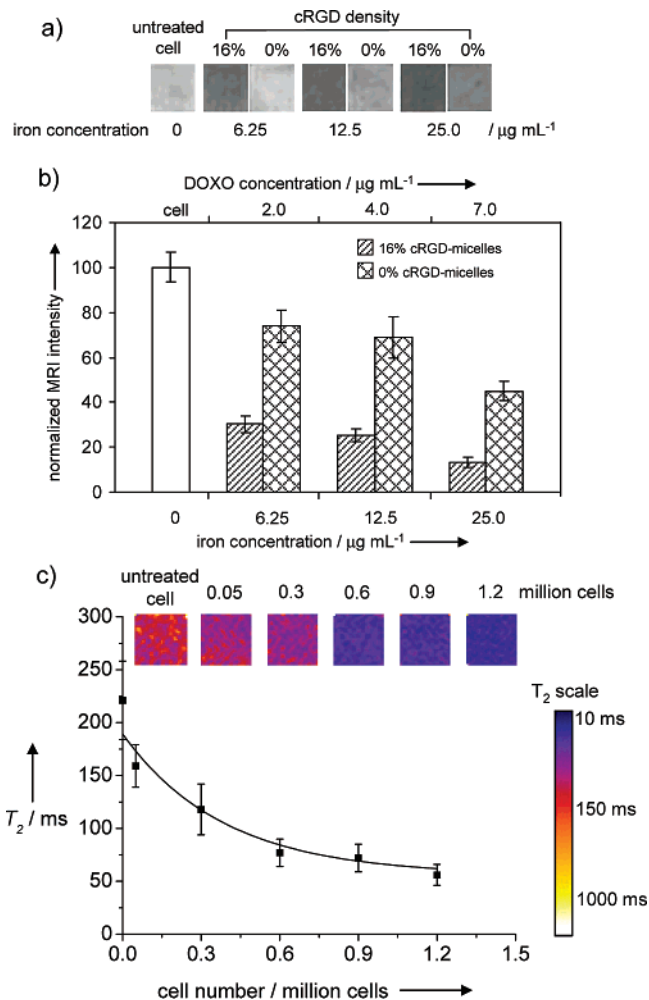
Figure 2. (a) T_2-weighted images (4.7 T, spin echo acquisition, TR = 6000 ms, TE = 90 ms) of untreated SLK cells, and SLK cells treated with 0% and 16% cRGD-DOXO-SPIO micelles at Fe concentrations of 6.25, 12.5, and 25 μg mL^{-1}. (b) MRI signal intensity of SLK cell samples described in Figure 2a as a function of Fe concentration (μg mL^{-1}). (c) T_2 values of SLK cells treated with 16% cRGD-DOXO-SPIO micelles as a function of cell number in the cell culture well. The inset shows T_2 maps of different cell samples.

%) that allows detection of micelles at nanomolar concentrations.[15] To investigate the $\alpha_v\beta_3$-targeting ability and MRI visibility of cRGD-SPIO-DOXO micelles, we chose tumor SLK endothelial cells with overexpression of $\alpha_v\beta_3$ integrin[16] in this study. The MRI signal magnitude of SLK cells was measured as a function of micelle doses of 0% and 16% cRGD micelles on a 4.7 T MRI scanner (Varian INOVA). Tumor SLK endothelial cells (1.8 × 10^6) were washed, trypsinized, and fixed after incubation with SPIO-loaded micelles at final Fe concentrations of 0, 6.25, 12.5, and 25 μg mL^{-1} in 10% FBS containing medium for 1 h. Cells were then mixed with 2% agarose solution in PBS and placed into wells of a 384-well plate. MR images were collected with conventional T_2-weighted spin echo acquisition parameters (TR = 6000 ms, TE = 90 ms). Uptake of SPIO nanoparticles inside SLK cells shortens the spin−spin relaxation time (T_2) by dephasing the spins of neighboring water protons and results in darkening of T_2-weighted images. Figure 2a shows

the MR images of wells containing SLK cells incubated with 16% and 0% cRGD micelles at the Fe concentrations of 0, 6.25, 12.5, and 25 μg mL^{-1}. Rapid and efficient $\alpha_v\beta_3$-mediated endocytosis led to significant darkening of MR images from cRGD-encoded micelles compared to cRGD-free micelles. More specifically, at 6.25 Fe μg/mL, the MRI signal intensity decreased from 73.8 ± 7.0 for non-cRGD micelles to 30.2 ± 3.5 for cRGD-encoded micelles. The untreated cells were used as a control with MR intensity at 100. Further decreases in MRI intensity were observed at the higher micelle doses for both cRGD-encoded and cRGD-free micelles, indicating the presence of a nonspecific uptake mechanism of micelles likely due to fluidic phase endocytosis.[17]

To further evaluate the T_2 values as a function of cell number, SLK cells incubated with 16% cRGD micelles (25 Fe μg mL^{-1}, 1 h) were systematically diluted from 1.2 to 0.05 million cells to a final volume 120 μL in each well. The T_2 values were measured and plotted versus cell number (Figure 2c). The control sample (1.2 million untreated cells) had a T_2 of 221 ± 37 ms, whereas the cells treated with cRGD-DOXO-SPIO micelles had T_2 values that decreased with an increase of cell number in each well (e.g., T_2 decreased from 159 ± 20 ms to 56 ± 10 ms for 0.05 to 1.2 million cells, respectively).

Flow cytometry and confocal laser scanning microscopy (CLSM) were used to evaluate the effect of cRGD on micelle targeting and uptake in $\alpha_v\beta_3$-expressing SLK tumor endothelial cells (derived from human Kaposi's sarcoma).[18] Figure 3a shows the mean fluorescence intensity after 0 and 16% cRGD micelles were incubated with SLK cells for 1 h. At micelle doses corresponding to 2, 5, and 10 μg/mL of DOXO, an approximate 2.5 fold increase in cell uptake was observed with 16% cRGD micelles over 0% cRGD micelles.

The uptake and intracellular distribution of these micelles were also evaluated by CLSM. The enhancement of cell uptake with 16% cRGD micelles (Figure 3e) over 0% cRGD micelles (Figure 3b) was in agreement with flow cytometry results. Rapid $\alpha_v\beta_3$-mediated endocytosis facilitated the internalization of cRGD-encoded micelles inside SLK cells. Once taken into cells, the majority of polymeric micelles were localized in cytoplasmic compartments (e.g., endosomes). Interestingly, higher concentrations of released DOXO were found in cell nuclei compared to that in a previous study using poly(ϵ-caprolactone) (PCL) as the core material.[12] The previous study showed that PCL segments can form crystalline regions in the micelle core, which may decrease the rate of DOXO release.[12] The use of poly(D,L-lactide), an amorphous polymer, as the core-forming material allows DOXO to easily diffuse through the polymer matrix for faster drug release. Moreover, because of the presence of the ionizable ammonium group on DOXO (p$K_a \approx 7$),[19] drug release rates appear to be pH-dependent (see the Supporting Information). At pH 5.0, 10.4% of drug was released in 6 h, approximately 6 times faster compared to 1.7% drug release at pH 7.4. The observed pH sensitivity is hypothesized to facilitate drug release from micelles once inside the acidic endosomal compartment and increase the
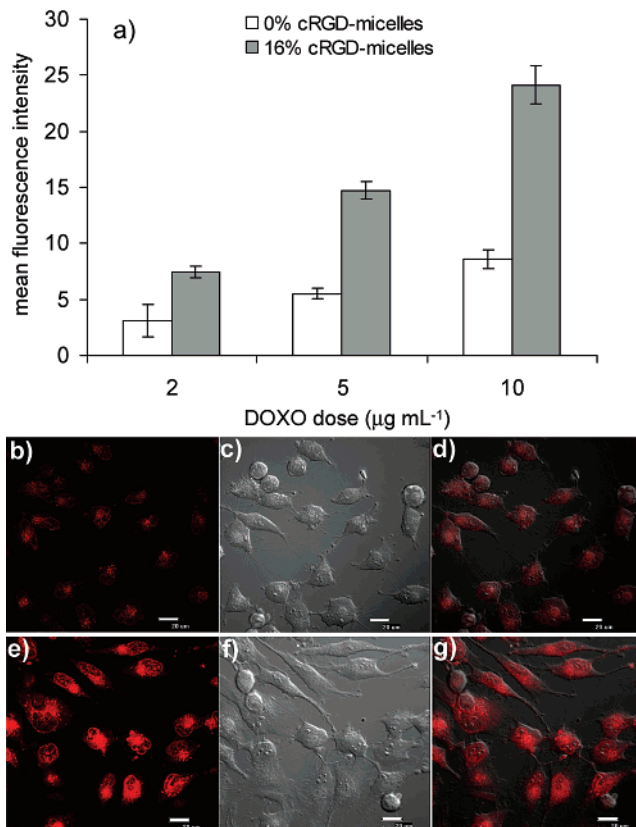
Figure 3. (a) Mean fluorescence intensity of SLK cells as a function of micelle dose (represented by DOXO concentration between 2 and 10 μg/mL) by flow cytometry. (b–g) Confocal laser scanning microscopy of DOXO fluorescence, DIC and merged images of DOXO fluorescence and DIC in SLK cells treated with 0% (b–d) and 16% cRGD (e–g) micelles after incubation for 1 h. DOXO fluorescent images were acquired at $\lambda_{ex} = 485$ nm and $\lambda_{em} = 595$ nm. The scale bars are 20 μm in all images.

intracellular bioavailability of the drug. DOXO accumulation inside the cell nucleus is necessary for its intercalation into DNA and interaction with topoisomerase II to cause DNA cleavage and cytotoxicity.[20]

Cytotoxicity studies with 0%, 5%, and 16% cRGD micelles and free DOXO (Figure 4) in SLK cells were carried out by a cell growth inhibition assay. Cells were treated for 1 h (Figure 4a) or 4 h (Figure 4b) with different micelle samples and then incubated for another 4 days. Percentage of cell growth (PG) was calculated as the ratio of the number of SLK cells of the treated group over the untreated control. Longer incubation times led to an overall decrease of cell viability for all of the micelle samples. Free DOXO showed the most effective inhibition of growth in both time points, consistent with the ease of the lipophilic drug to cross cell membranes and reach its enzymatic target in the nucleus (data not shown). The 16% cRGD micelles without DOXO was used as a control and showed no significant growth inhibition, indicating minimal cell cytotoxicity due to the polymer micelle carriers alone. In comparison, DOXO-loaded micelles showed different degrees of cytotoxicity. The values of PG after 4 h incubation decreased from $42.8 \pm 2.0\%$ (0% cRGD) and $30.8 \pm 6.6\%$ (5% cRGD) to $7.0 \pm 1.4\%$ (16% cRGD), demonstrating the effect of cRGD on the cytotoxicity.
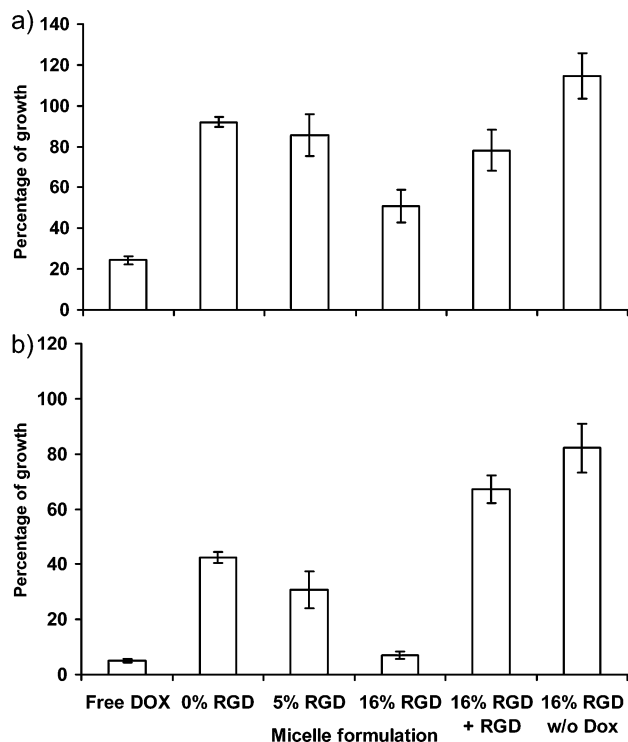
Figure 4. Inhibition of SLK cell growth in the presence of different formulations of SPIO-loaded micelles with or without 1 μM DOXO concentration after (a) 1 h or (b) 4 h incubation times. The percent inhibition of cell growth was calculated as the ratio of cell number in the treated sample divided by that in the untreated control. Error bars were obtained from triplicate samples.

Preincubation of SLK cells with free cRGD peptide significantly reduced the cytotoxic response of SLK cells to 16% cRGD-DOXO-SPIO micelles (PG: $67.1 \pm 5.0\%$), supporting the $\alpha_v\beta_3$-dependent growth inhibition. In the current micelle design, encapsulation of DOXO and SPIO nanoparticles inside the hydrophobic micelle cores has the advantages of avoiding potential exposure of hydrophobic SPIO surfaces and adsorption of blood proteins. In addition, polymer chain entanglement led to a very low critical micelle concentration (CMC) at ~12 μg/mL.[7] All of the experiments in the current study were performed at concentrations much higher than the CMC to ensure the integrity of micelles. "Stealth" micelles with similar PEG–PLA copolymer compositions have demonstrated significantly increased in vivo half-lives of drugs (e.g., paclitaxel) to 11 h in cancer patients.[21] The increased in vivo stability should enhance the effectiveness of these cRGD-functionalized micelles for active targeting to tumor vasculature. Current work is in progress to evaluate the in vivo efficacy of the cRGD-DOXO-SPIO micelles in an animal tumor model.

In summary, multifunctional polymeric micelles were developed to provide effective targeting to $\alpha_v\beta_3$-integrin receptors, ultrasensitive detection by MRI, and growth inhibition in tumor SLK cells. This integrated nanomedicine platform will open many exciting opportunities for the targeted delivery of therapeutic agents to cancerous tumors as well as the use of MRI as a noninvasive strategy to monitor tumor targeting efficiency to improve the therapeutic outcome of drug therapy.

Supporting Information Available: Syntheses of amphiphilic copolymers and SPIO nanoparticles; preparation and characterization of cRGD-encoded, DOXO-SPIO-encapsulated micelles are provided. This material is available free of charge via the Internet at http://pubs.acs.org.

References

(1) Li, K. C.; Pandit, S. D.; Guccione, S.; Bednarski, M. D. *Biomed. Microdevices* **2004**, *6*, 113−6.
(2) Moghimi, S. M.; Hunter, A. C.; Murray, J. C. *FASEB J.* **2005**, *19*, 311−30.
(3) Kwon, G. S. *Crit. Rev. Ther. Drug Carrier Syst.* **2003**, *20*, 357−403.
(4) Otsuka, H.; Nagasaki, Y.; Kataoka, K. *Adv. Drug Delivery Rev.* **2003**, *55*, 403−419.
(5) Torchilin, V. P. *J. Controlled Release* **2001**, *73*, 137−72.
(6) Danson, S.; Ferry, D.; Alakhov, V.; Margison, J.; Kerr, D.; Jowle, D.; Brampton, M.; Halbert, G.; Ranson, M. *Br. J. Cancer* **2004**, *90*, 2085−91.
(7) Shuai, X.; Ai, H.; Nasongkla, N.; Kim, S.; Gao, J. *J. Controlled Release* **2004**, *98*, 415−26.
(8) Matsumura, Y.; Hamaguchi, T.; Ura, T.; Muro, K.; Yamada, Y.; Shimada, Y.; Shirao, K.; Okusaka, T.; Ueno, H.; Ikeda, M.; Watanabe, N. *Br. J. Cancer* **2004**, *91*, 1775−81.
(9) Yamamoto, Y.; Nagasaki, Y.; Kato, Y.; Sugiyama, Y.; Kataoka, K. *J. Controlled Release* **2001**, *77*, 27−38.
(10) Varner, J. A.; Cheresh, D. A. *Curr. Opin. Cell Biol.* **1996**, *8*, 724−30.
(11) Hood, J. D.; Bednarski, M.; Frausto, R.; Guccione, S.; Reisfeld, R. A.; Xiang, R.; Cheresh, D. A. *Science* **2002**, *296*, 2404−7.
(12) Nasongkla, N.; Shuai, X.; Ai, H.; Weinberg, B. D.; Pink, J.; Boothman, D. A.; Gao, J. *Angew. Chem., Int. Ed.* **2004**, *43*, 6323−7.
(13) Sun, S.; Zeng, H. *J. Am. Chem. Soc.* **2002**, *124*, 8204−5.
(14) Shuai, X. T.; Ai, H.; Nasongkla, N.; Kim, S.; Gao, J. M. *J. Controlled Release* **2004**, *98*, 415−426.
(15) Ai, H.; Flask, C.; Weinberg, R.; Shuai, X.; Pagel, M.; Farrell, D.; Duerk, J.; Gao, J. *Adv. Mater.* **2005**, *17*, 1949−1952.
(16) Rader, C.; Popkov, M.; Neves, J. A.; Barbas, C. F., III. *FASEB J.* **2002**, *16*, 2000−2.
(17) Savic, R.; Luo, L.; Eisenberg, A.; Maysinger, D. *Science* **2003**, *300*, 615−8.
(18) Samaniego, F.; Young, D.; Grimes, C.; Prospero, V.; Christofidou-Solomidou, M.; DeLisser, H. M.; Prakash, O.; Sahin, A. A.; Wang, S. *Cell Growth Differ.* **2002**, *13*, 387−95.
(19) Burke, T. G.; Morin, M. J.; Sartorelli, A. C.; Lane, P. E.; Tritton, T. R. *Mol. Pharm.* **1987**, *31*, 552−6.
(20) Zunino, F.; Capranico, G. *Anti-Cancer Drug Des.* **1990**, *5*, 307−17.
(21) Kim, T. Y.; Kim, D. W.; Chung, J. Y.; Shin, S. G.; Kim, S. C.; Heo, D. S.; Kim, N. K.; Bang, Y. J. *Clin. Cancer Res.* **2004**, *10*, 3708−3716.

NL061412U